Materials Research Letters

ISSN: (Print) 2166-3831 (Online) Journal homepage: https://www.tandfonline.com/loi/tmrl20

Simultaneously increasing strength and ductility of nanoparticles reinforced Al composites via accumulative orthogonal extrusion process

Jun Liu, Zhe Chen, Fengguo Zhang, Gang Ji, Mingliang Wang, Yu Ma, Vincent Ji, Shengyi Zhong, Yi Wu & Haowei Wang

To cite this article: Jun Liu, Zhe Chen, Fengguo Zhang, Gang Ji, Mingliang Wang, Yu Ma, Vincent Ji, Shengyi Zhong, Yi Wu & Haowei Wang (2018) Simultaneously increasing strength and ductility of nanoparticles reinforced Al composites via accumulative orthogonal extrusion process, Materials Research Letters, 6:8, 406-412, DOI: 10.1080/21663831.2018.1471421

To link to this article: https://doi.org/10.1080/21663831.2018.1471421

MATER. RES. LETT.
2018, VOL. 6, NO. 8, 406–412
https://doi.org/10.1080/21663831.2018.1471421

MATERIALS RESEARCH LETTERS
Taylor & Francis
Taylor & Francis Group

ORIGINAL REPORT

Simultaneously increasing strength and ductility of nanoparticles reinforced Al composites via accumulative orthogonal extrusion process

Jun Liu[a], Zhe Chen[a], Fengguo Zhang[a], Gang Ji[b], Mingliang Wang[c], Yu Ma[b,d], Vincent Ji[d], Shengyi Zhong[c], Yi Wu[c] and Haowei Wang[a]

[a]State Key Laboratory of Metal Matrix Composites, Shanghai Jiao Tong University, Shanghai, People's Republic of China; [b]Unité Matériaux et Transformations, CNRS UMR 8207, Université de Lille, Lille, France; [c]School of Materials Science and Engineering, Shanghai Jiao Tong University, Shanghai, People's Republic of China; [d]ICMMO-UMR 8182, Université Paris-Sud, Orsay, France

ABSTRACT

Ceramic particles have been introduced into metal matrices to improve the strength and stiffness of metals, albeit at the cost of the ductility unfortunately. Simultaneously increasing the strength and ductility of metal matrix composites (MMCs) is still a challenge. Accumulative orthogonal extrusion process (AOEP), which disperses nanoparticles and refines grain structures of particles reinforced MMCs via severe plastic deformation, is proposed in this paper. The high strength (687 MPa) and superior ductility (14.8%) are simultaneously achieved in the resultant TiB_2 particles reinforced Al–Zn–Mg–Cu matrix composites, and the underlying mechanisms are discussed in terms of particles' influences.

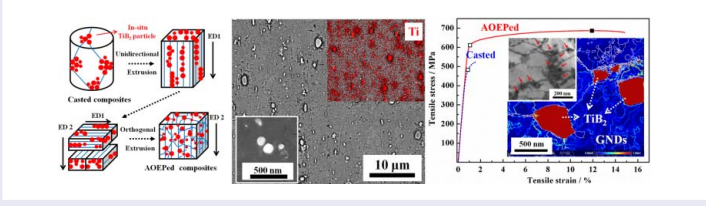

ARTICLE HISTORY
Received 27 March 2018

KEYWORDS
Metal matrix composites; nanocomposites; severe plastic deformation; mechanical properties; ductility

IMPACT STATEMENT

An easily realized SPD technology is proposed to effectively optimize the structures of nanoparticles reinforced composites in industrial scale. High strength and good ductility are simultaneously achieved in the resultant composites.

In the past decades, particulate reinforced metal matrix composites (Particle-MMCs) have developed to be one of the potential structural materials due to their high strength and stiffness. Many kinds of micron sized particles, such as SiC [1], B_4C [2], Al_2O_3 [3], are introduced in metal matrices to improve the strength and Young's modulus of the materials albeit at the cost of the ductility. Thus, new technologies are proposed to simultaneously increase the strength and ductility of MMCs. Recently, Chen et al [4] successfully introduced uniform nanoparticles into metal matrices, and the final nanocomposites presented ultrahigh strength and good plasticity as well. It has demonstrated that uniformly distributed nano-reinforcements can simultaneously improve the strength and ductility of MMCs. Specifically, in the Al-based composites, the novel nano-sized reinforcements such as carbon nanotubes (CNTs) [5, 6], graphene nanosheets (GNSs) [7, 8] and nanoparticles (nano-TiB_2, nano-SiC, etc) [9, 10] are added in Al matrices aiming at further improved mechanical performance. Although these efforts have been performed to a certain extent, the ultrahigh strength ($\sigma_{0.2} > 600$ MPa) and good ductility ($\varepsilon > 10\%$) are still rarely obtained concurrently in Al-based nanocomposites.

Clustering is one of the major problems in nanoparticles reinforced MMCs (NanoP-MMCs), especially when the composites are fabricated via solidification process [11]. Nanoparticles tend to be pushed by the

CONTACT Zhe Chen zhe.chen@sjtu.edu.cn State Key Laboratory of Metal Matrix Composites, Shanghai Jiao Tong University, Shanghai, 200240, People's Republic of China; Yi Wu eagle51@sjtu.edu.cn School of Materials Science and Engineering, Shanghai Jiao Tong University, Shanghai, 200240, People's Republic of China

Supplemental data for this article can be accessed here. https://doi.org/10.1080/21663831.2018.1471421

solidification front and therefore cluster at the grain boundaries in the casted NanoP-MMCs [12]. Although the plastic deformations such as hot extrusion [13] and rolling [14] have been utilized to optimize the microstructures of NanoP-MMCs, where the strains are not effective to disperse the clusters of nanoparticles. Thereafter, the severe plastic deformation (SPD) techniques which impose extremely high strains, including equal channel angular pressing [15], high pressure torsion [16], are employed and can neither uniform the nanoparticles completely. Only the friction stir processing (FSP) [17] has been proved capable of well dispersing the nanoparticles in NanoP-MMCs, but FSP usually introduces flaws like pores in materials [18]. Furthermore, all these SPD processes are particularly demanding and limited in work-piece size, therefore it is difficult to be widely applied in producing bulk NanoP-MMCs in industry. Herein, an easy-to-use SPD technology with large processing size is eagerly needed to optimize the structures of bulk NanoP-MMCs.

In this study, an easily realized accumulative orthogonal extrusion process (AOEP) is innovatively proposed to disperse the clusters of nanoparticles in the in-situ synthesized NanoP-MMCs. It is found that the novel AOEP processes can effectively disperse the nanoparticles and refine the grain structures in composites. The resultant bulk NanoP-MMCs have a high strength of 687 MPa as well as a good ductility of 14.8%.

The NanoP-MMCs in this study are 6 wt.% nano-TiB_2 particles reinforced Al–6.9Zn–2.3Mg–2.4Cu alloys (nominal in wt.%) matrix composites (Nano-TiB_2/Al–Zn–Mg–Cu). The composites were firstly fabricated using an in-situ mixed salt method, as described in [19]. According to our former study [20], the TiB_2 particles in Al matrices display a wide size distribution from several nanometers to hundreds of nanometers, but with a dominant fraction at the nanoscale (< 100 nm). Figure 1(b) is the micrograph of the in-situ casted Nano-TiB_2/Al–Zn–Mg–Cu composites showing that TiB_2 particles agglomerate at grain boundaries to form clusters with alloy elements segregations.

The as-casted composites were processed by a novel AOEP technology involving two steps of *unidirectional extrusion* and the subsequent *orthogonal extrusion* (Figure 1(a)). Details of the processing procedures are provided in the supplemental materials (Figure S1). Figure 1(c) is the micrograph of unidirectionally extruded composites, and it shows that the former TiB_2 particles clusters have been transformed to parallel bands of particles along the unidirectional extrusion direction (ED 1). Figure 1(d) exhibits the TiB_2 particles distributions in composites after orthogonal extrusion, showing the

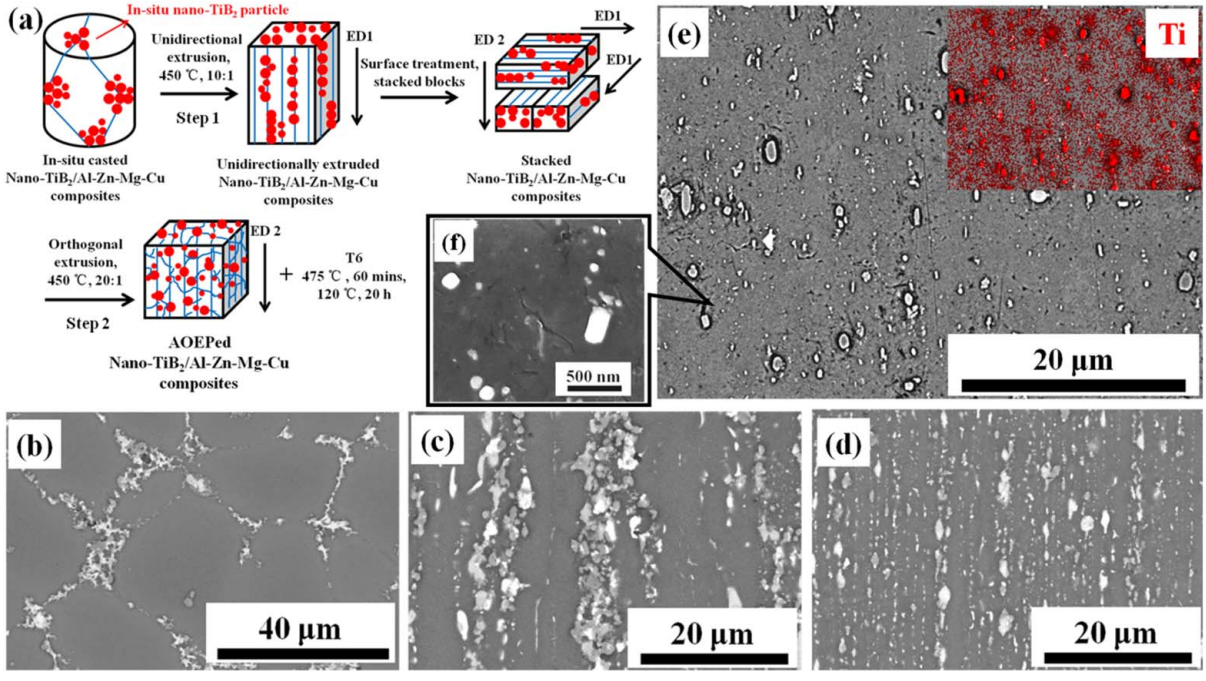

Figure 1. (a) The flow process chart of AOEP in this study. The SEM images of Nano-TiB_2/Al–Zn–Mg–Cu composites in (b) in-situ casted state, (c) unidirectional extrusion and (d) AOEPed state, correspondingly. (e) SEM micrograph of AOEPed Nano-TiB_2/Al–Zn–Mg–Cu composites after T6 treatment and the inset gives the corresponding Ti element distribution in EDX. (f) is the enlarged SEM image showing the details of nano-TiB_2 particles.

dispersion of the formerly clustered TiB_2 particles in Al matrices.

The AOEPed composites were subjected to solid-solution at 475°C for 60 mins, quenched in water and aged at 120°C for 20 h (T6 treatment) before the tensile tests. The dog-bone tensile test specimens were machined along the orthogonal extrusion direction (ED 2) with gauge length of 2 mm × 3 mm × 10 mm, and tensile tests were carried out on a Zwick/Roell machine at a strain rate of 10^{-4}/s and 10^{-3}/s at room temperature. A TESCAN MAIA3 scanning electron microscope (SEM), equipped with a BRUKER e-Flash^{HR} electron backscatter diffraction (EBSD) detector and energy dispersive X-ray spectroscopy (EDX), was used for studying the distributions of TiB_2 particles and grain structures of Al matrices in composites. Geometrically necessary dislocations (GNDs) maps in composites after tensile tests were estimated from the automated crystal orientation mapping (ACOM), acquired by a FEI Tencai G2 transmission electron microscope, operated at 200 kV and equipped with a Nanomega Astar precession unite (TEM/ASTAR). An electron probe size of around 1–2 nm and a step size of 5 nm were used to reveal the nanoscale characteristics. The matrix alloys were fabricated by the same processes as a counterpart, whose grain structures and mechanical properties were also identified as above.

Figure 1(e) is the SEM micrograph of AOEPed composites after T6, where the corresponding Ti element distribution in EDX map is given by the inset. The enlarged image (Figure 1(f)) gives the details of nano-TiB_2 particles. The result shows the two-step AOEP technology can effectively disperse the TiB_2 particles and promote the dissolution of alloy elements segregations (Figures S2 and S3) in the resultant composites.

Figure 2(a, c) shows the grain structures of Al matrices after AOEP, which consist of short ribbon grains and fine equiaxial grains, and detailed grain evolutions during AOEP are given in Figure S4. The inset in Figure 2(a) is the corresponding grain size distribution of Al matrices with an average grain size of 2.0 μm, which is much finer than the grain structures (6.8 μm) of AOEPed matrix alloys (Figure S5). Figure 2(b, d) gives the resultant grain structures of composites after T6 treatment. The grain structures still consist of ribbon grains and embedded equiaxial grains, and the grains have only slightly grown to an average grain size of 2.8 μm. Therefore, besides of dispersing nanoparticles, the AOEP refines the Al matrices as well. The uniformly redistributed TiB_2 particles can effectively hinder the migrations of grain boundaries and inhibit the grain coarsening during the subsequent heat treatment.

Figure 3(a) is the tensile strain–stress curve of the Nano-TiB_2/Al–Zn–Mg–Cu composites. It shows that the as-casted composites after T6 treatment exhibit a yield strength (YS) of only 482 MPa and fracture at a strain below 2%. After AOEP, much higher YS of 610 MPa, ultimate strength (UTS) of 687 MPa and good ductility of 14.8% are concurrently achieved in the resultant composites (Figure S6). Figure 3(b) compares the mechanical properties of the AOEPed Nano-TiB_2/Al–Zn–Mg–Cu composites with those of other Al matrix MMCs in literatures [1, 2, 5, 7, 8, 21–33]. It shows that the AOEPed Nano-TiB_2/Al–Zn–Mg–Cu composites have nearly twofold strength over those of the reported Particle-MMCs and GNSs-MMCs exhibiting comparable ductility. Moreover, its ductility is almost twice as high as that of NanoP-MMCs with the equivalent strength. Consequently, the mechanical behavior of composites in this study stands out from the trend, suggesting a superior combination of mechanical properties with enhanced toughness as the nanostructure-hierarchy Al alloys with known mechanical performance boundaries [34]. The mechanical properties of the AOEPed matrix alloys (609 MPa and 12.6%) are also given in Figure 3(b), which are much lower than those of AOEPed composites. Thus, the superior mechanical properties of resultant composites are mainly stem from the influences of TiB_2 particles.

First of all, the uniform nano-TiB_2 particles contribute predominantly to the high strength of AOEPed composites through the Orowan mechanism [4]:

$$\Delta\sigma_{\text{Orowan}} = \frac{\phi G_m b}{d_p}\left(\frac{6V_p}{\pi}\right)^{1/3}, \tag{1}$$

where G_m, b, V_p and d_p are the shear modulus of the matrix, the Burgers vector, the volume fraction and the size of nanoparticles, correspondingly. ϕ is a constant equal to 2. Considering that in this study, $G_m = 28$ GPa, $b = 0.283$ nm, $V_p = 0.022$ and $d_p = 33$ nm [20], the $\Delta\sigma_{\text{Orowan}}$ offered by TiB_2 is estimated to be 167 MPa, which is much higher than the increased strength (120 MPa) from coarse-grain 7XXX alloys to UFG 7XXX alloys [35]. Apart from the nano-TiB_2 particles, fine grain structures, solid-solution and second phase nano-precipitates (Figure S7) strengthening in Al–Zn–Mg–Cu matrices contribute to strengthen the composites. Thus, although the composites fabricated in this study have coarser grain structures (2.8 μm) than the SPDed 7XXX Al alloys with UFG (< 1 μm) structures or nanocrystallines (< 100 nm), the composites are stronger than most of the SPDed 7XXX Al alloys, as shown in Figure 3(b).

A good ductility is also obtained in AOEPed Nano-TiB_2/Al–Zn–Mg–Cu composites, which could be mainly attributed to two factors:

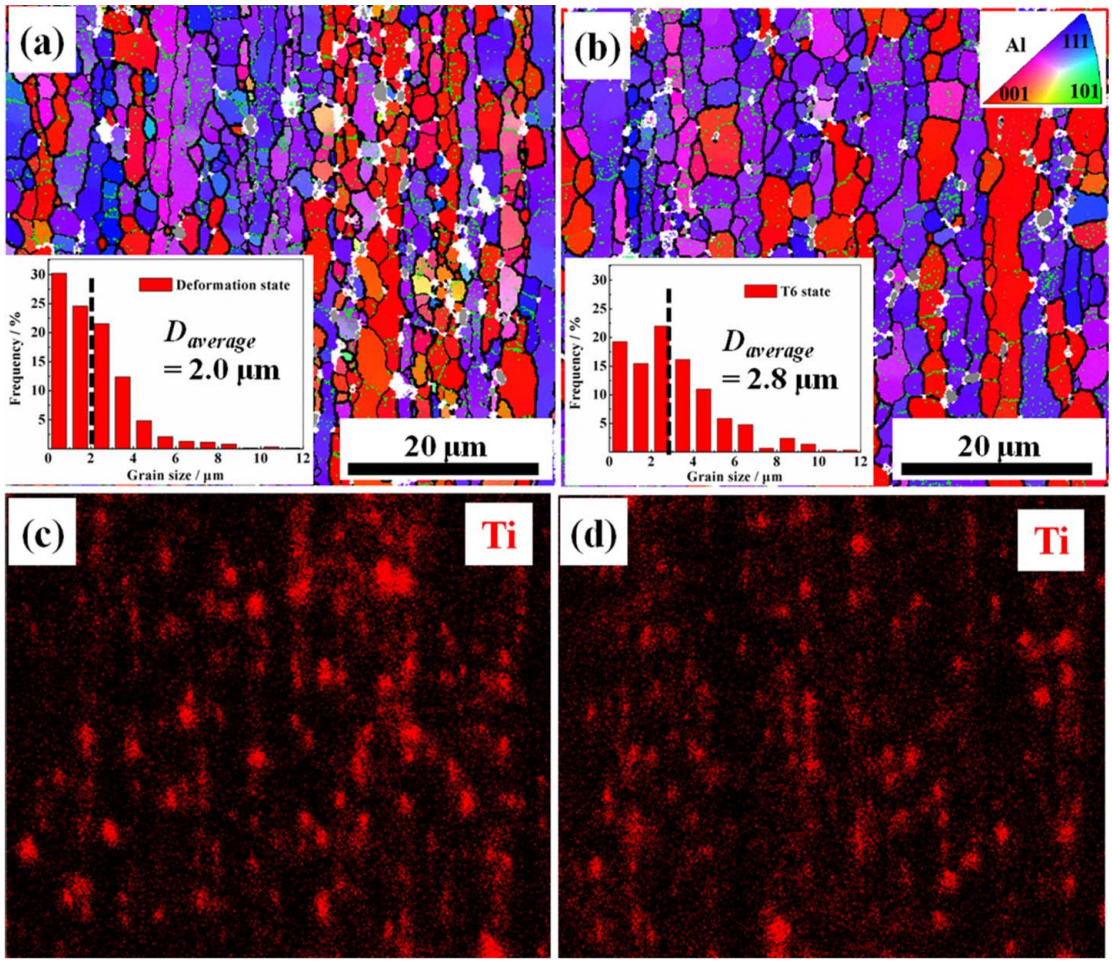

Figure 2. EBSD maps of AOEPed Nano-TiB_2/Al–Zn–Mg–Cu composites in (a) deformation state and (b) T6 state, the insets depict the corresponding grain size distribution of composites and the statistic average grain sizes are also given by labels. High angle grain boundaries ($\theta > 15°$) are marked in thick black lines, while low ($5° < \theta < 15°$) and very low ($2° < \theta < 5°$) angle grain boundaries are marked in thin black and lime green lines, correspondingly. The color codes representing the crystal orientation in IPF images are also given in (b). (c) and (d) are the corresponding Ti element distributions in EDX of (a) and (b).

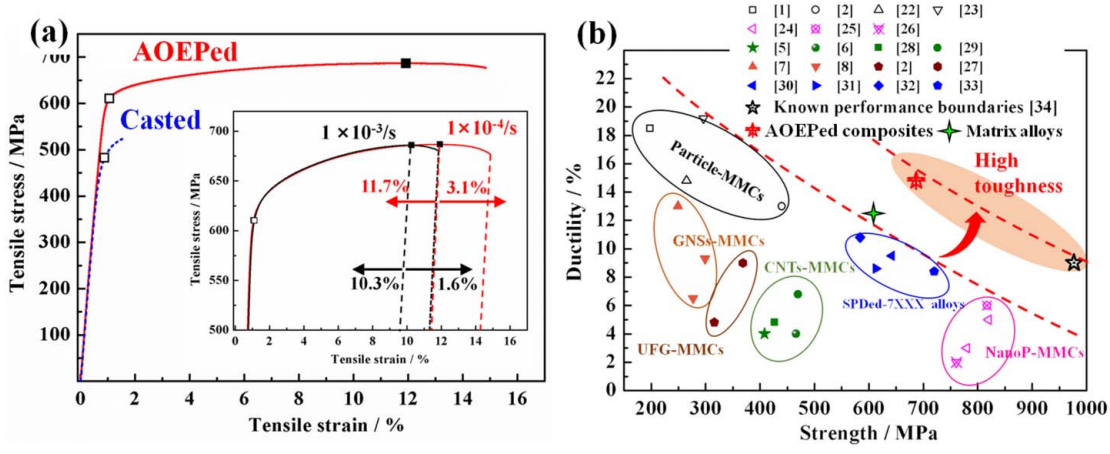

Figure 3. (a) The tensile strain–stress curves of the Nano-TiB_2/Al–Zn–Mg–Cu composites. The hollow square is the 0.2% offset yield point and black solid square is the ultimate strength point. The inset compares the elongations of composites at a strain rate of 10^{-3}/s and 10^{-4}/s. (b) Strength versus tensile ductility of the AOEPed composites and matrix alloys, other Al-based MMCs and SPDed 7XXX alloys in literatures.

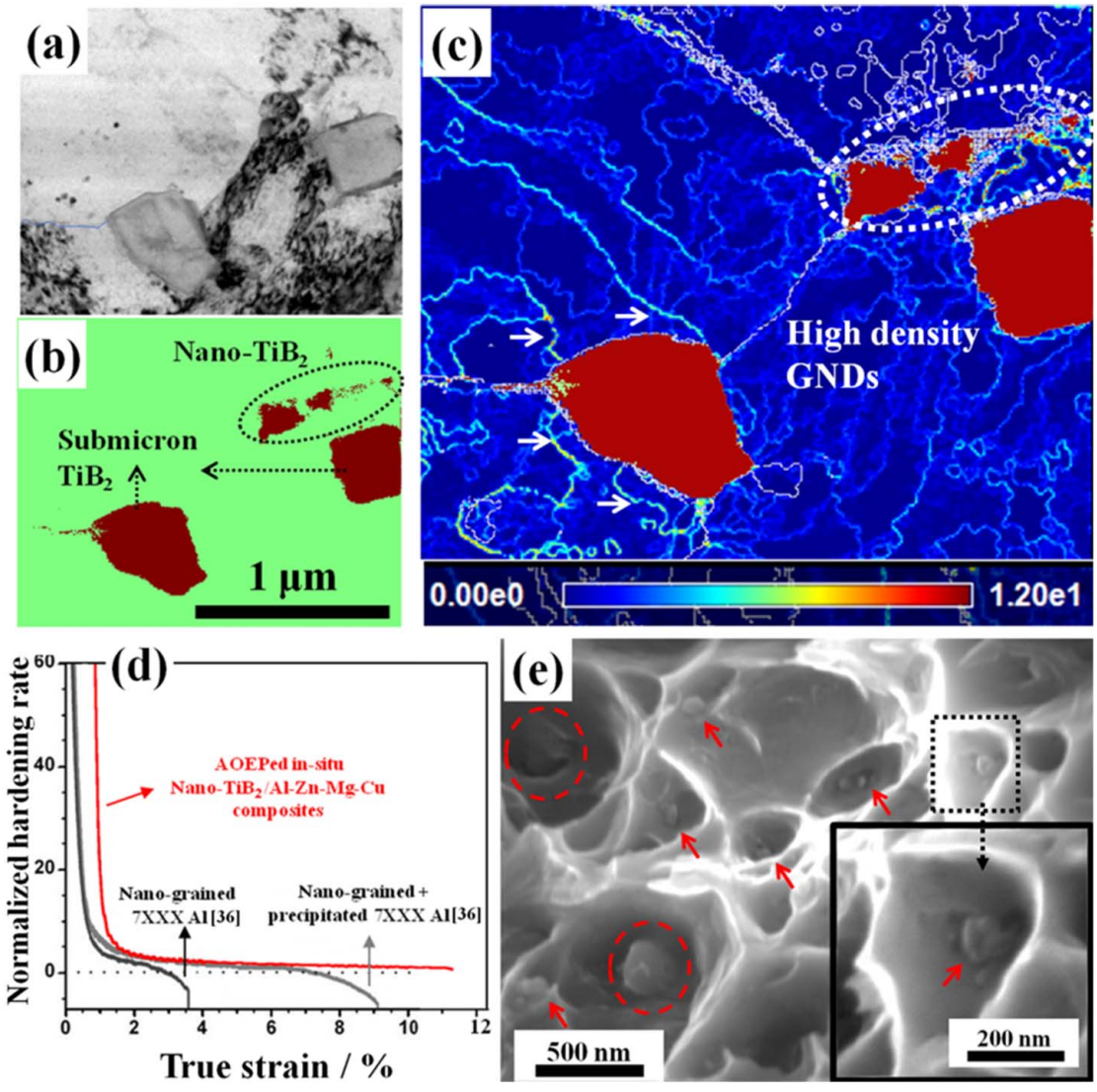

Figure 4. (a) TEM image of Nano-TiB_2/Al–Zn–Mg–Cu composites after tensile tests. (b) is the corresponding phases map of (a). (c) is the corresponding GNDs map of (a), and the white dash circle and arrows indicate regions with high GNDs densities surrounding TiB_2 particles. (d) The normalized work-hardening rate of Nano-TiB_2/Al–Zn–Mg–Cu composites and reported 7XXX alloys with true strains. (e) SEM fracture surface images of Nano-TiB_2/Al–Zn–Mg–Cu composites, red dash circles and red arrows point out the submicron and nano-TiB_2 particles in dimples respectively.

(1) A high work-hardening rate. Figure 4(a–c) demonstrates the structures and GNDs distributions in the composite samples after tensile tests from TEM/ASTAR analysis. It can be seen that both submicron and nano-TiB_2 particles in matrices can effectively trap the dislocations (Figures 4(c) and S7). A large amount of dislocations are notably accumulated around these TiB_2 particles in Al matrices during plastic deformation (Figures 4(a) and S7), which will result in a better work-hardening rate. A high work-hardening rate can delay localized deformation (necking) under tensile stress and is essential for the good uniform elongation [36]. Figure 4(d) shows the normalized work-hardening rate of AOEPed Nano-TiB_2/Al–Zn–Mg–Cu composites with true strains, and the comparison with the normalized work-hardening rate of nano-grained 7XXX alloys [36]. It shows that the AOEPed composites have the highest work-hardening rate, and therefore exhibit a large uniform elongation of 11.7%. Figure 4(e) shows the fracture surface of AOEPed Nano-TiB_2/Al–Zn–Mg–Cu composites. The fracture surface consists of deep and small dimples, with both submicron TiB_2 particles (red dash circles) and dense nano-TiB_2 particles (red arrows) located in the cores of dimples. This result further confirms that the dislocations have been accumulated around these particles during plastic deformation

as discussed above, finally inducing ductile fracture (Figure S8).

(2) The great strain rate sensitivity. The inset in Figure 3(a) gives the uniform and post-necking elongations of AOEPed Nano-TiB_2/Al–Zn–Mg–Cu composites at strain rate of 10^{-3} /s and 10^{-4} /s respectively, which illustrates that the composites exhibit a twofold elongation after necking at the slower strain rate. This result indicates that the AOEPed Nano-TiB_2/Al–Zn–Mg–Cu composites have a great strain rate sensitivity, contributing to the resultant post-necking ductility as well [37].

In summary, the newly proposed AOEP technology is proved effective to disperse the clusters of in-situ synthesized nanoparticles in MMCs and refine the grain structures of matrices. Both high strength (687 MPa) and good ductility (14.8%) are achieved in the resultant composites. Combined with a high Young's modulus of 78 GPa (Figure S6), our composites are a desirable lightweight material for situations where both strength and ductility are highly demanded. It is also noteworthy that the AOEP is repeatable (Figure S1) and can be iterated to further refine the grain structures and modify the mechanical properties of MMCs. Moreover, the novel AOEP technology offers the possibility of achieving industrially bulk SPDed samples by conventional extrusion facilities, so it is promising to be applied to process other NanoP-MMCs in industry.

Disclosure statement

No potential conflict of interest was reported by the authors.

Funding

This work was supported by the National Natural Science Foundation of China [Nos. 51201099, 51301108].

ORCID

Vincent Ji http://orcid.org/0000-0003-1979-7323

References

[1] Slipenyuk A, Kuprin V, Milman Y, et al. Properties of P/M processed particle reinforced metal matrix composites specified by reinforcement concentration and matrix-to-reinforcement particle size ratio. Acta Mater. 2006;54(1):157-166. doi:10.1016/j.actamat.2005.08.036

[2] Kai X, Li Z, Fan G, et al. Strong and ductile particulate reinforced ultrafine-grained metallic composites fabricated by flake powder metallurgy. Scr Mater. 2013;68(8):555-558. doi:10.1016/j.scriptamat.2012.11.024

[3] Jiang L, Li Z, Fan G, et al. A flake powder metallurgy approach to Al2O3/Al biomimetic nanolaminated composites with enhanced ductility. Scr Mater. 2011;65(5):412-415. doi:10.1016/j.scriptamat.2011.05.022

[4] Chen LY, Xu JQ, Choi H, et al. Processing and properties of magnesium containing a dense uniform dispersion of nanoparticles. Nature. 2015;528(7583):539-543. doi:10.1038/nature16445. PubMed PMID: 26701055.

[5] Liu ZY, Xiao BL, Wang WG, et al. Singly dispersed carbon nanotube/aluminum composites fabricated by powder metallurgy combined with friction stir processing. Carbon NY. 2012;50(5):1843-1852. doi:10.1016/j.carbon.2011.12.034

[6] Xu R, Fan G, Tan Z, et al. Back stress in strain hardening of carbon nanotube/aluminum composites. Materials Research Letters. 2018;6(2):113-120. doi:10.1080/21663831.2017.1405371

[7] Wang J, Li Z, Fan G, et al. Reinforcement with graphene nanosheets in aluminum matrix composites. Scr Mater. 2012;66(8):594-597. doi:10.1016/j.scriptamat.2012.01.012.

[8] Zhao M, Xiong D-B, Tan Z, et al. Lateral size effect of graphene on mechanical properties of aluminum matrix nanolaminated composites. Scr Mater. 2017;139:44-48. doi:10.1016/j.scriptamat.2017.06.018

[9] Kwon H, Kawasaki A, Leparoux M. Mechanical behaviour of dual nanoparticle-reinforced aluminium alloy matrix composite materials depending on milling time. J Compos Mater. 2017;51(25):3557-3562. doi:10.1177/0021998316673521

[10] Li XP, Ji G, Chen Z, et al. Selective laser melting of nano-TiB_2 decorated AlSi10Mg alloy with high fracture strength and ductility. Acta Mater. 2017;129:183-193. doi:10.1016/j.actamat.2017.02.062. PubMed PMID: WOS:000400033900018.

[11] Tjong SC. Novel nanoparticle-reinforced metal matrix composites with enhanced mechanical properties. Adv Eng Mater. 2007;9(8):639-652. doi:10.1002/adem.200700106

[12] Xu JQ, Chen LY, Choi H, et al. Theoretical study and pathways for nanoparticle capture during solidification of metal melt. J Phy Condens Matter. 2012;24(25):255304. doi:10.1088/0953-8984/24/25/255304. PubMed PMID: 22640981.

[13] Chen Z, Sun GA, Wu Y, et al. Multi-scale study of microstructure evolution in hot extruded nano-sized TiB_2 particle reinforced aluminum composites. Mater Des. 2017;116:577-590. doi:10.1016/j.matdes.2016.12.070

[14] Dan CY, Chen Z, Ji G, et al. Microstructure study of cold rolling nanosized in-situ TiB_2 particle reinforced Al composites. Mater Des. 2017;130:357-365. doi:10.1016/j.matdes.2017.05.076

[15] Sabirov I, Kolednik O, Valiev RZ, et al. Equal channel angular pressing of metal matrix composites: effect on particle distribution and fracture toughness. Acta Mater. 2005;53(18):4919-4930. doi:10.1016/j.actamat.2005.07.010.

[16] Phuong DD, Trinh PV, An NV, et al. Effects of carbon nanotube content and annealing temperature on the hardness of CNT reinforced aluminum nanocomposites processed by the high pressure torsion technique. J Alloys Compd. 2014;613:68-73. doi:10.1016/j.jallcom.2014.05.219

[17] Chen Z, Li J, Borbely A, et al. The effects of nano-sized particles on microstructural evolution of an in-situ TiB_2/6063Al composite produced by friction stir processing. Mater Des. 2015;88:999-1007. doi:10.1016/j.matdes.2015.09.127

[18] Ju X, Zhang F, Chen Z, et al. Microstructure of multi-pass friction-stir-processed Al-Zn-Mg-Cu alloys reinforced by nano-sized TiB2 particles and the effect of T6 heat treatment. Metals (Basel). 2017;7(12). doi:10.3390/met7120530. PubMed PMID: WOS:000419184500015.

[19] Ma SM, Zhang P, Ji G, et al. Microstructure and mechanical properties of friction stir processed Al–Mg–Si alloys dispersion-strengthened by nanosized TiB_2 particles. J Alloys Compd. 2014;616:128-136. doi:10.1016/j.jallcom.2014.07.092

[20] Tang Y, Chen Z, Borbély A, et al. Quantitative study of particle size distribution in an in-situ grown Al–TiB_2 composite by synchrotron X-ray diffraction and electron microscopy. Mater Charact. 2015;102:131-136. doi:10.1016/j.matchar.2015.03.003

[21] Zhang SL, Shi XX, Zhao YT, et al. Preparation, microstructures and mechanical properties of in-situ (TiB_2 + ZrB_2)/AlSi9Cu3 composites. J Alloys Compd.2016;673:349-357. doi:10.1016/j.jallcom.2016.02.243

[22] Kai X, Tian K, Wang C, et al. Effects of ultrasonic vibration on the microstructure and tensile properties of the nano ZrB 2 /2024Al composites synthesized by direct melt reaction. J Alloys Compd. 2016;668:121-127. doi:10.1016/j.jallcom.2016.01.152

[23] Wei H, Li Z, Xiong D-B, et al. Towards strong and stiff carbon nanotube-reinforced high-strength aluminum alloy composites through a microlaminated architecture design. Scr Mater. 2014;75:30-33. doi:10.1016/j.scriptamat.2013.11.014

[24] Li M, Ma K, Jiang L, et al. Synthesis and mechanical behavior of nanostructured Al 5083/n-TiB_2 metal matrix composites. Mater Sci Eng: A. 2016;656:241-248. doi:10.1016/j.msea.2016.01.031

[25] Jiang L, Yang H, Yee JK, et al. Toughening of aluminum matrix nanocomposites via spatial arrays of boron carbide spherical nanoparticles. Acta Mater. 2016;103:128-140. doi:10.1016/j.actamat.2015.09.057

[26] Xu R, Tan Z, Xiong D, et al. Balanced strength and ductility in CNT/Al composites achieved by flake powder metallurgy via shift-speed ball milling. Composites Part A: Appl Sci Manuf. 2017;96:57-66. doi:10.1016/j.compositesa.2017.02.017

[27] Alizadeh M. Comparison of nanostructured Al/B4C composite produced by ARB and Al/B4C composite produced by RRB process. Mater Sci Eng: A. 2010;528(2):578-582. doi:10.1016/j.msea.2010.08.093

[28] Stein J, Lenczowski B, Fréty N, et al. Mechanical reinforcement of a high-performance aluminium alloy AA5083 with homogeneously dispersed multi-walled carbon nanotubes. Carbon NY. 2012;50(6):2264-2272. doi:10.1016/j.carbon.2012.01.044

[29] Nam DH, Cha SI, Lim BK, et al. Synergistic strengthening by load transfer mechanism and grain refinement of CNT/Al–Cu composites. Carbon NY. 2012;50(7):2417-2423. doi:10.1016/j.carbon.2012.01.058

[30] Panigrahi SK, Jayaganthan R. Effect of ageing on microstructure and mechanical properties of bulk, cryorolled, and room temperature rolled Al 7075 alloy. J Alloys Compd. 2011;509(40):9609-9616. doi:10.1016/j.jallcom.2011.07.028

[31] Senkov ON, Shagiev MR, Senkova SV, et al. Precipitation of Al3(Sc,Zr) particles in an Al–Zn–Mg–Cu–Sc–Zr alloy during conventional solution heat treatment and its effect on tensile properties. Acta Mater. 2008;56(15):3723-3738. doi:10.1016/j.actamat.2008.04.005

[32] Li B, Pan Q, Huang X, et al. Microstructures and properties of Al–Zn–Mg–Mn alloy with trace amounts of Sc and Zr. Mater Sci Eng: A. 2014;616:219-228. doi:10.1016/j.msea.2014.08.024

[33] Zhao YH, Liao XZ, Jin Z, et al. Microstructures and mechanical properties of ultrafine grained 7075 Al alloy processed by ECAP and their evolutions during annealing. Acta Mater. 2004;52(15):4589-4599. doi:10.1016/j.actamat.2004.06.017

[34] Liddicoat PV, Liao XZ, Zhao Y, et al. Nanostructural hierarchy increases the strength of aluminium alloys. Nat Commun. 2010;1:63. doi:10.1038/ncomms1062. PubMed PMID: 20842199.

[35] Ma K, Wen H, Hu T, et al. Mechanical behavior and strengthening mechanisms in ultrafine grain precipitation-strengthened aluminum alloy. Acta Mater. 2014;62:141-155. doi:10.1016/j.actamat.2013.09.042

[36] Zhao YH, Liao XZ, Cheng S, et al. Simultaneously increasing the ductility and strength of nanostructured alloys. Adv Mater. 2006;18(17):2280-2283. doi:10.1002/adma.200600310

[37] Zhao Y, Topping T, Bingert JF, et al. High tensile ductility and strength in bulk nanostructured nickel. Adv Mater. 2008;20(16):3028-3033. doi:10.1002/adma.200800214